



This is a repository copy of *Porous hydroxyapatite-bioactive glass hybrid scaffolds fabricated via ceramic honeycomb extrusion*.

White Rose Research Online URL for this paper:
<http://eprints.whiterose.ac.uk/135270/>

Version: Accepted Version

Article:

Elbadawi, M., Wally, Z.J. and Reaney, I.M. orcid.org/0000-0003-3893-6544 (2018) Porous hydroxyapatite-bioactive glass hybrid scaffolds fabricated via ceramic honeycomb extrusion. *Journal of the American Ceramic Society* , 101 (8). pp. 3541-3556. ISSN 0002-7820

<https://doi.org/10.1111/jace.15514>

Reuse

Items deposited in White Rose Research Online are protected by copyright, with all rights reserved unless indicated otherwise. They may be downloaded and/or printed for private study, or other acts as permitted by national copyright laws. The publisher or other rights holders may allow further reproduction and re-use of the full text version. This is indicated by the licence information on the White Rose Research Online record for the item.

Takedown

If you consider content in White Rose Research Online to be in breach of UK law, please notify us by emailing eprints@whiterose.ac.uk including the URL of the record and the reason for the withdrawal request.



eprints@whiterose.ac.uk
<https://eprints.whiterose.ac.uk/>

Porous Hydroxyapatite-Bioactive Glass Hybrid Scaffolds Fabricated via Ceramic Honeycomb Extrusion

M. Elbadawi^{1,2*}, Zena. J. Wally³ and Ian Reaney³

¹ Department of Mechanical Engineering, University of Sheffield, Sheffield, S1 3JD, United Kingdom.

² Pharmaceutical and Biomaterials Research Group, Division of Medical Sciences, Department of Health Sciences, Luleå University of Technology, Luleå 97187, Sweden

³ Department of Materials Science and Engineering, University of Sheffield, Sir Robert Hadfield Building, Sheffield S1 3JD, UK

*Corresponding author, email: elbadawi.moe@gmail.com

Abstract

The successful fabrication of hydroxyapatite-bioactive glass scaffolds using honeycomb extrusion is presented herein. Hydroxyapatite was combined with either 10 wt% stoichiometric Bioglass® (BG1), calcium-excess Bioglass® (BG2) or canasite (CAN). For all composite materials, glass-induced partial phase transformation of the HA into the mechanically weaker β -tricalcium phosphate (TCP) occurred but XRD data demonstrated that BG2 exhibited a lower volume fraction of TCP than BG1. Consequently, the maximum compressive strength observed for BG1 and BG2 were 30.3 ± 3.9 and 56.7 ± 6.9 MPa, respectively, for specimens sintered at 1300 °C. CAN scaffolds, in contrast, collapsed when handled when sintered below 1300 °C, and thus failed. The microstructure illustrated a morphology similar to that of BG1 sintered at 1200 °C, and hence a comparable compressive strength (11.4 ± 3.1 MPa). The results highlight the great potential offered by honeycomb extrusion for fabricating high-strength porous scaffolds. The compressive strengths exceed that of commercial scaffolds, and biological tests revealed an increase in cell viability over seven days for all hybrid scaffolds. Thus it is expected that the incorporation of 10 wt% bioactive glass will provide the added advantage of enhanced bioactivity in concert with improved mechanical stability.

Keywords: Honeycomb Extrusion; Scaffold; Hydroxyapatite; Bioglass; Canasite; Composite.

1 Introduction

Porous synthetic bone scaffolds continue to be a subject of great interest. These are used in the treatment of orthopaedic abnormalities, and can be derived either naturally (autograft, allograft or xenograft) or synthetically¹. Traditionally, autografts and allografts are used, but these are associated with disease transmission, poor histocompatibility, limited availability and high costs²⁻⁴. Synthetic bone graft substitutes (BGS) overcome the aforementioned complications, and hence, have been extensively studied over the past few decades. In addition, there are several synthetic materials that possess bioresorbable properties that preclude the need for a second operation, thereby halving surgery-associated risks⁵.

The ideal BGS should be bioactive, porous and mechanically sound^{6, 7}. Ceramic honeycomb extrusion is a technique capable of achieving porous ceramic BGS with compressive strengths comparable to that of cortical bone⁸, which has seldom been achieved by both traditional and contemporary fabrication techniques used to fabricate BGS. In addition, honeycomb extrusion is unique in that it offers controlled and interconnected porosity, fabrication of large-sized scaffolds and is industrially scalable^{9, 10}. In spite of these advantageous, the technique has not been widely adopted for BGS. As such, honeycomb extrusion has only been used to fabricate hydroxyapatite (HA)⁸ or β -tricalcium phosphate (β -TCP)¹⁰. Although honeycomb extrusion was successful in fabricating these materials with mechanical properties exceeding that of traditional methods (i.e. > 20 MPa), their respective biological properties were not optimized.

In light of HA's biological limitation, the state of the art in scaffold fabrication encompasses a multi-material approach, with emphasis on hybridising materials from different classes. The aim therein is to deliver a BGS that overcomes undesirable biological behaviour

of calcium phosphates. A common hybridising approach is to combine HA or β -TCP with 45S5 Bioglass® (BG)^{11, 12}, which is amongst the most widely researched and clinically used biomaterials. BG possesses exceptional bioactivity, and indeed its addition to HA and β -TCP has been shown to improve bioactivity^{11, 12}. This was attributed to the chemical composition of BG, whereby the dissolution of ions elicits a response that results in bioactivity within minutes of in vivo implantation. Furthermore, the addition of bioactive glasses have been demonstrated to improve the compressive strengths of HA. This is achieved through liquid-phase sintering, whereby the glass melts and through capillary forces and particle rearrangement, enhances the densification of HA¹³⁻¹⁶. Therefore, the rationale for incorporating glass is to enhance both the biological and mechanical properties.

Glasses containing CaO-P₂O₅ are generally considered as bioactive because of their analogous elemental composition to the inorganic component of bone¹⁷. Canasite (CAN) is one such example. In its glass-ceramic form, canasite demonstrates exceptional mechanical properties in comparison to BG^{18, 19}. Furthermore, canasite contains fluorine and potassium that are prevalent as trace ions in bone²⁰, but are not found in 45S5 BG. Moreover, the fluorine results in a fluorapatite layer forming in vivo that is more chemically stable than a hydroxyapatite layer observed in BG¹¹. Despite these exceptional properties, the material has not been studied as a hybrid with HA.

The current study progresses the application of honeycomb extrusion by demonstrating its versatility for the fabrication of porous ceramic-glass hybrid materials by combining HA with three bioactive glasses: either stoichiometric BG, calcium-excess BG or canasite. The hybrid scaffolds were then shaped and sintered at 1200, 1250 and/or 1300 °C, and subsequently characterized for their chemical, physical and biological properties.

2 Experimental Procedure

2.1 Raw Materials

Hydroxyapatite powder (Purum grade, Sigma Aldrich, UK) was produced by calcining at 1000 °C for five hours prior to mixing. The bioactive glasses were prepared using the melt-quenching technique. All precursor reagents were purchased from Glassworks Services (Doncaster, UK) except the calcium fluoride (analytical grade, Fisher Scientific, UK) and the ammonium dihydrogen phosphate (analytical grade, Acros Organics, UK). Before melting the precursors, the powders were dried overnight in an oven, and then mixed using the high-shear energy mixer for homogenisation and de-agglomeration. Batches of 250 g were melted in a mullite crucible at 1450 °C in air for 4 hours. The melt was quenched in distilled water and casted as frit. The frit was then crushed and ground into fine glass powder using an in-house percussion mortar, planetary mill (Fritsch, Germany) and an attrition mill (Union Process®, USA). **Table 1** enumerates the oxide composition used for all three glasses.

2.2 Fabrication Process

Clay-like pastes were formulated using Methocel™ (Trademark of Dow Chemical Company, USA) and distilled water as additives. Initially, the HA and bioactive glass powders were mixed together using the high-shear energy mixer for ten minutes (Speedmixer™ DAC 300 FVZ, Synergy Devices, UK). The binder was added thereafter and mixed for a further five minutes. Lastly, distilled water was added, wherein mixing continued until an extrudable paste was formulated. **Table 2** lists the paste composition used for all samples.

Porous scaffolds were fabricated using an in-house extruder and honeycomb die. The extruder die geometry and extrusion speed have been previously reported in Ref²¹. Prior to extrusion, the pastes were vacuumed and compacted in situ. A servo-hydraulic press was used to actuate the piston using a controller (SmarTest ONE, MOOG, USA). Once extruded, the

green bodies were allowed to dry overnight before transferred to a muffle furnace (Elite Thermal Systems Ltd, UK) for de-binding and sintering. De-binding was performed at 1 °C/min to a maximum temperature of 400 °C. A multi-stage temperature procedure was used to sinter the extrudates. First, the extrudates were sintered at 5 °C/min until 600 °C, followed by a heating rate of 1 °C/min until 800 °C after which a dwell of one hour was applied, before ramping to either 1200, 1250 or 1300 °C at a rate of 5 °C/min followed by a dwell period of eight hours, and a cooling rate of 2.5 °C/min. The extrudates were then sectioned into 4.1 x 4.1 x 4.5 cm³ scaffolds for optical analysis, and quantitative measurements of bulk porosity and compressive strength.

2.3 Characterisation

2.3.1 Particle Characterisation

The bioactive glass powders were characterized for their density, surface area and particle size. Powder density measurements were performed using a helium pycnometer (Accupyc 1340, Micromeritics, UK). A multipoint BET Surface analysis was performed using a surface characterizer (3Flex, Micromeritics, UK); and the results were inspected for evidence of experimental errors as detailed in Ref. ²². Particle size analysis was conducted using a particle size analyzer (Mastersizer 3000, Malvern, UK), where all samples were subjected to vigorous ultrasound prior to measurements. In addition, simultaneous thermal analysis (STA) (SDT-Q6000, TA Instruments, UK) was employed to elucidate the thermal characteristics of the raw powders. The thermal behaviour of the bioactive glass is key to defining a sintering profile for the hybrid extrudates. Samples were poured into an alumina pan, and analysed in air with a flow rate of 100 ml/min.

2.3.2 Chemical Analyses

Powdered samples were characterized using X-ray fluorescence (XRF) (Zetium, Panalytical, UK), X-ray diffraction (XRD) (D5000, Siemens, UK) and Fourier-transformation-infrared spectroscopy (FTIR) (Frontier, Perkin Elmer, UK). For FTIR, samples were ground with potassium bromide and pressed into disks, using a stainless steel die, prior to analysis at a ratio of 2:200 mg. For chemical analyses of sintered scaffolds, samples were ground crushed and ground into fine powder, and thoroughly mixed.

2.3.3 Microscopy

Scanning electron microscopy (SEM) (Inspect F50, FEI, USA) was used to observe the microstructural features on gold-coated samples. Optical microscopy (BA310Met-T, Miotic) was also employed to examine macro-pore size and strut thickness.

2.3.4 Scaffold Characterisation

The scaffolds were characterized with respect to their chemical properties using XRD and FTIR, as detailed in 2.3.2. The scaffolds were ground into fine powder using first a stainless steel percussion mortar, followed by an agate pestle and mortar prior to analysis. Scaffold bulk porosity was measured using the helium pycnometer described in 2.3.1. The protocol used and the derived porosity calculation has been previously detailed²³. Compression tests were carried-out using a universal testing machine (Roell, Zwick, UK) fitted with a 20 kN load cell (Xforce K, Zwick; 0.5% resolution) at a rate of 1 mm/min. Compression loading was performed parallel to the cell alignment.

2.3.5 Cell Viability

Cell viability tests were performed on discoid pellets of the hybrid materials. Samples were prepared using a stainless steel die press, and subsequently sintered in muffle furnace. Once sintered, the samples were then autoclaved at a temperature of 121 °C for thirty minutes prior to commencing the cell viability. The protocol can be found in the Appendix 1.

3 Results and Discussion

3.1 Raw Material Properties

The aim of the comminution procedure was to attain particle sizes below 100 μm . This would ensure that the glass particles can traverse the narrowest gap within the honeycomb die (500 μm). Furthermore, smaller particle sizes would ensure better dispersion of glass particles within the HA powders, and consequently mitigate heterogeneous densification. Moreover, this has to be achieved without significant contamination from the milling media. The following section details the raw glass powder properties with regards to particle, chemical and thermal properties.

3.1.1 Powder Properties

Powder properties are known to affect the final scaffold properties, and thus, it is necessary to note the powder characteristics. **Table 3** enumerates the particle properties with regards to size, density and surface area. As demonstrated, the comminution approach used was successful in reducing the particle sizes to below 100 μm . In doing so, the powder densities varied from 2.63 to 2.75 g/cm^3 , similar to those previously reported for BG²⁴. Furthermore, the surface area ranged from 2.25 to 3.57 m^2/g . **Fig. 1** portrays the morphology of the glass particles following comminution.

3.1.2 Chemical Properties

X-ray Fluorescence (XRF) was used to detect the elemental composition of the powders once ground, where calcium, sodium, silicon, phosphor and aluminium were detected; and fluoride and potassium for canasite glass. XRF of the milled glass powders revealed minor compositional changes during glass melting, wherein dissolution of aluminium from the crucible had occurred. However, no compositional variation was observed due to milling. XRD

analysis of the raw glass powders was also conducted, and the results are presented in **Fig. 2**. All samples displayed an amorphous hump and no crystalline phases.

Fig. 3 depicts the FTIR results of the raw powders. The BG samples displayed similar spectra, with silica bands detected at 1035, 930, 745, 502 cm^{-1} ; and a phosphate band at 605 cm^{-1} . Silica bands in the canasite were detected at 1040, 777 and 470 cm^{-1} , and a phosphate band between 606-575 cm^{-1} . Therefore, FTIR analyses corroborated with the XRD in demonstrating the absence of crystallinity in all glass powders.

3.1.3 Thermal Properties

Simultaneous thermal analysis (STA) was employed to determine the melting points for the glasses in order to achieve liquid-phase sintering. **Fig. 4** outlines the STA thermograms, which comprised differential scanning calorimetry (DSC) and thermal gravimetric analysis (TGA). Melting of the glass manifested in the form of a sharp endothermic peak at approximately 1200 °C in DSC. Furthermore, a transient mass loss was observed that coincided with the DSC endotherm, which was attributed to the loss of phosphate in all samples²⁵ and silicon tetrafluoride in CAN^{25, 26} during melting. TGA also determined that the final mass loss was <2 wt%, which was attributed to said volatiles and dehydration.

The STA data revealed the melting points of BG1, BG2 and CAN, which were 1158, 1183 and 1230 °C, respectively. The difference in melting properties of BG1 and BG2 were due to the latter possessing less sodium oxide concentration, which is a known fluxing agent used to reduce the melting temperature of glass networks²⁷. The reduction thereof in BG2 thus mitigated the fluxing effect. Therefore, the substitution of 5 wt% CaO for Na₂O resulted in a more thermally stable material. From the STA data, it was decided that BG1 and BG2 hybrids would be sintered at 1200, 1250 and 1300 °C to obtain liquid phase sintering; whereas CAN hybrids would be sintered at 1250 and 1300 °C as melting commenced above 1200 °C.

In summary, crystalline-free Bioglass® and Canasite powders were successfully synthesized using the melt-quenching approach, and subsequently ground. The comminution steps resulted in particle sizes suitable for extrusion without producing significant contamination. STA data revealed that BG2 was more thermally stable than BG1, however both melted at <1200 °C. Canasite on the other hand exhibited the highest melting temperature, which precluded it from being sintered at 1200 °C.

3.2 Scaffold Properties

HA scaffolds with 10 wt% glass were successfully extruded, and sintered at different temperatures. Canasite samples sintered at 1250 °C cracked when handled. Hence, only the complete data of the CAN samples sintered at 1300 °C are reported. **Fig. 5** are various images of the fashioned CAN sample.

3.2.1 Chemical Structure

3.2.1.1 XRD

XRD analyses of sintered scaffolds are illustrated in **Fig. 6** and **Fig. 7**. All samples exhibited a biphasic calcium phosphate (CaP) composition comprising β -tricalcium phosphate (β -TCP) (PDF: 04-001-7104) and HA (PDF: 01-089-4405). In addition, traces of calcium silicate (CaSiO_3) (PDF: 04-010-0710) were detected.

In BG1, β -TCP peaks were more dominant than HA, and remained so in samples sintered at 1300 °C, but their dominance gradually diminished with increasing sintering temperature. As **Fig. 6(b)** illustrates, the large peaks pertaining to β -TCP and HA at 31 and 31.6°, respectively, were comparable in intensity. BG2, in contrast, exhibited comparable β -TCP and HA peak intensities when sintered at 1200 °C, with the HA phases dominating when sintered at 1250 and 1300 °C (**Fig. 6(a)**). Furthermore, BG2 exhibited more intense peaks

associated with a CaSiO_3 phase which increased in intensity with increasing sintering temperature.

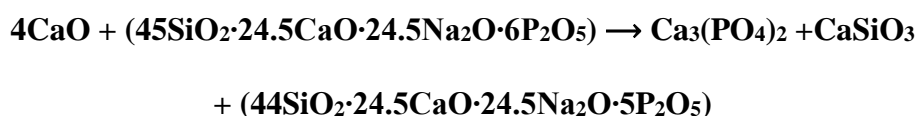
Fig. 7 depicts the XRD pattern of canasite hybrid scaffolds sintered at 1250 and 1300 °C. The results are akin to BG1, wherein the β -TCP dominated over HA, and traces of CaSiO_3 (CS) were observed. As mentioned, scaffolds sintered at 1250 °C fractured when handled, however the XRD data was included to highlight the reduction in β -TCP phase with increasing temperature, which is again mirrored by increases to HA and CaSiO_3 peaks.

Phase transformation of HA in the presence of bioactive glass into β -TCP have been previously documented²⁸⁻³¹. HA is known to decompose into anhydrous calcium phosphate phases at elevated temperatures³², however, this was not believed to be the case herein. On the contrary, increasing the sintering temperature favoured HA phase formation. **Thus, it was concluded that the addition of glass induced the phase transformation, as opposed to a temperature-induced phase transformation.**

The bioactive glass-induced phase transformation can be ascribed to the imbalance in calcium concentration between HA and glass; whereby a concentration gradient was established across the two phases. Calcium, in the form of calcium oxide, diffused from the hydroxyapatite into the glassy phase, which is relatively deficient in calcium. The following established reaction³³ was proposed:



In addition, the calcium oxide could further react with the phosphate and silica group from the glass to yield more β -TCP and calcium silicate, respectively:



This reaction also explains why hybrids containing BG2 exhibited a lower concentration of TCP. BG2, with a higher CaO concentration than BG1 and CAN, alleviated the diffusion gradient and hence reduced the driving force for Ca^{2+} to migrate from the HA. Therefore, it can be concluded that increasing the calcium oxide quantity in a glass will mitigate the phase transformation to TCP in HA-bioactive glass hybrids. Moreover, decreasing the surface area by sintering at higher temperatures may also reduce the interfacial region over which the calcium can migrate from the HA. This could explain why with increasing sintering temperature a decrease in β -TCP intensity was observed. This behaviour has been previously noted by other researchers^{15, 29}.

3.2.1.2 FTIR

FTIR analysis of the hybrid samples are outlined in **Fig. 8** and **Fig. 9**, wherein functional groups pertaining to β -TCP and HA were detected. In BG1 and BG2, phosphate bands pertaining to β -TCP were observed at 1120, 1080, 1043, 945, 604 and 553 cm^{-1} ^{34, 35}; whereas those associated with HA were detected at 1010, 980, 590 and 565 cm^{-1} ; a hydroxyl group indicative of HA was detected at 3570 cm^{-1} in 1200 and 1250 $^{\circ}\text{C}$ ³⁶.

FTIR analyses of CAN-HA only detected phosphate bands of β -TCP, and a hydroxyl group at 3530 cm^{-1} . Phosphates associated with HA and β -TCP share similar band positions, and in concert with a relatively poorly defined spectra, made it difficult to discern between the two. XRD analyses of HA-CAN highlighted that β -TCP was the more dominant phase, and hence the bands ascribed to this phase.

3.2.2 Physical and Mechanical Properties

Optical microscopy was utilized to determine the macro-pore size achieved (i.e. the extruded channels). These ranged from 750-940 μm , which are greater than the desirable sizes for

scaffolds³⁷, thus providing enhanced nutrient transport and cell attachment for facilitating bone ingrowth³⁸.

Fig. 10 (a) depicts the bulk porosity values for all the samples, which is the total porous volume of the scaffolds. The volume porosity of BG1 scaffolds sintered at 1200 °C was 71.6 ± 1.11 vol%, which decreased to 61.8 ± 0.9 and 59.6 ± 1.0 vol% when the sintering temperature was raised to 1250 and 1300 °C, respectively. Bulk porosity values for BG2 scaffolds were generally lower than their BG1 equivalent, with values of 61.9 ± 0.7 , 57.1 ± 1.3 and 55.0 ± 0.6 vol% obtained for scaffolds sintered at 1200, 1250 and 1300 °C, respectively. The canasite scaffolds sintered at 1300 °C possessed a bulk porosity of 62.3 ± 0.8 vol%.

3.2.3 Microstructure

Following compression testing, the microstructure of fractured hybrid scaffolds were investigated using SEM (**Fig. 11** and **Fig. 12**). The mode of fracturing was mixed in all samples, consisting of both inter- and transgranular fractures. Furthermore, a highly micro-porous morphology was described, with pore sizes of $< 10 \mu\text{m}$, which can facilitate protein adsorption³⁹,⁴⁰. The micrographs revealed small sintering necks had formed between adjacent HA grains in the BG samples sintered at 1200 °C. The morphology presented with an appearance that is similar to the initial stage of sintering⁴¹, despite using high temperatures. Increasing the sintering temperatures to 1250 and 1300 °C proceeded to densify the scaffolds, however, complete densification was not attained, [as previously achieved by the author](#)²³. Nevertheless, it was evident that the improved compressive strengths with increasing sintering temperature was a reflection of the microstructural densification.

The CAN scaffolds sintered at 1300 °C presented with similar neck sizes to that of BG1 sintered at 1200 °C, which explains why hybrids thereof possessed the weakest compressive strength in all samples sintered at 1300 °C. Thus it could be inferred the scaffolds sintered

below 1300 °C did not coalesce. This could also be the reason why the HA-CAN samples sintered at 1250 °C failed. Further experiments will need to be conducted to elucidate the cause of the poor densification of HA and CAN in comparison to BG¹⁵.

Santos et al. (1994) investigated both CaO-P₂O₅ binary glass systems and BG²⁹. In contrast to CaO-P₂O₅ binary glass, the authors reported an increase in TCP phase with the incorporation of BG, and surmised the presence of sodium in BG expedited hydroxyapatite decomposition, and hence hindered densification. This is in agreement with the present study, whereby a decrease in Na content increased densification. Bellucci et al. (2013) compared the 40 wt% addition of both CaO-excess and stoichiometric BG. The authors reported the latter, which possessed a markedly higher Na content, to result in a greater densification when sintered at 1150 °C⁴². Hence, the effects of Na may differ depending on the ratio of HA to BG. Moreover, the substitution of Si into HA may have also influenced the latter's densification, as Si has been revealed to lower the sintered density of HA^{43,44}. Therefore, it can be reasoned that reducing either Si and/or Na in BG will enhance densification of HA-BG hybrids. However, the inclusion of both Na and Si are required for achieving desirable biological properties. Thus, said consequences must be considered during the design process.

One approach in reducing the effects of Si- or Na-induced decomposition is to decrease the proportion of bioactive glass content within the composite. Indeed, previous studies have shown small quantities of CaO-P₂O₅ binary glass yielded enhanced densification relative to pure HA. However, Tancred et al. (2001) investigated the addition of BG content ranging from 2.5 to 50 wt% and reported a decrease in densification compared to pure HA, with further decreases observed at higher glass content⁴⁵. Furthermore, Knowles et al. (1996) also observed a decrease in densification with the addition of 2 wt% Na₂O-CaO-P₂O₅ glass¹⁵. Thus, decreasing the BG content in this study may have provided no benefits to densification.

From **Table 5**, it is evident that a longer dwell time was used in the present study in comparison to previous work. An extended dwell time was expected to provide sufficient time for the glass melt to wet the ceramic particles and achieve liquid phase sintering. This was not attained herein, and hence it can be concluded that a long dwell time provided no benefits. On the other hand, an increase in densification with increasing temperature was achieved, which is in agreement with previous studies that reported similar trends^{13, 15, 29}. Increase in temperature progresses ceramic densification, however, it can also increase glass reactivity, which suppresses densification. As mentioned in section **3.2.1.1**, it is possible that the HA particles achieved a higher degree of sintering at increasing temperatures, thereby reducing the interfacial area prior to glass melt wetting and, hence, reducing the rate of decomposition. Knowles et al. (1996) observed increases in density with increasing temperature until 1350 °C, whereat significant β -TCP lead to expansion in the material. Therefore, increasing sintering temperature is one method of achieving greater densification, provided the threshold for thermal-induced HA decomposition is not exceeded.

3.2.4 Mechanical Properties

Fig. 10 (b) depicts the corresponding maximum compressive strength values attained for the hybrid scaffolds when the load was applied parallel to the cell direction. The results illustrated that BG1 samples achieved values of 9.8 ± 1.7 , 24.1 ± 3.3 and 30.3 ± 3.9 MPa when processed at 1200, 1250 and 1300 °C, respectively; whereas, BG2 samples achieved 16.7 ± 1.1 , 48.4 ± 5.2 and 56.7 ± 6.9 MPa, at identical sintering temperatures. Sintering the canasite scaffold at 1300 °C resulted in a value of 11.4 ± 3.1 MPa, which was considerably lower than either BG samples.

Ceramic honeycomb extrusion has been demonstrated to produce porous scaffolds with remarkable compressive strengths⁴⁶, and the present study provides further credence thereto. The compressive strengths recorded herein are considerably greater than pure HA scaffolds that are commercially available, such as the BGS Endobon®⁴⁷. Furthermore, the addition of 10 wt% bioactive glass will expedite the slow bioactivity of HA. Therefore, taking these facets into consideration, the hybrid scaffolds fabricated herein are an excellent alternative to Endobon®. Moreover, the compressive strengths are exceptional given that they are comparable to that attained for dense HA-bioactive glass^{13, 48, 49}. With regards to commercial hybrid BGS, the results are once more favourable. Bonelike®, which is a promising material that displays enhanced bioactivity with regards to standard HA, is composed of HA reinforced with 4 wt% bioactive glass, and is suitable for direct clinical use¹¹. This was confirmed when Bonelike® was implanted in the tibia of 13 patients during osteotomy surgery, with the aim of treating the medial compartment osteoarthritis of the knee⁵⁰. Though the porosity values are similar, hitherto the compressive strengths reported for Bonelike® are 2 MPa with pore sizes of approximately 100 μm ⁵¹. Therefore, comprised of a higher glass composition and remarkably greater compressive strengths, it can be concluded that honeycomb extruded hybrid scaffolds used for similar clinical applications will result in superior biological and mechanical performances.

It should be remarked that the compressive strengths obtained herein were lower than what has been obtained for pure HA scaffolds by extrusion^{46, 52}. This decrease was attributed to the presence of β -TCP, where the addition thereof to HA has been reported to mechanically weaken scaffolds^{53, 54}. The current study adds further credence to this by illustrating that a bioactive glass composition capable of suppressing phase transformation of HA yielded higher compressive strengths, as observed in the HA-BG2 hybrid. In addition, BG2 exhibited relatively higher calcium silicate peaks, which has been previously reported to enhance the

compressive strength of HA scaffolds^{55, 56}. Similarly, Desogus et al. (2015)⁵⁷ found that CaO-rich Bioglass® improved the mechanical properties of dense hybrids compared to stoichiometric BG, with higher Vickers hardness and elastic modulus recorded. Therefore, it can be inferred that increasing the CaO ratio improves the mechanical properties of hybrid scaffolds.

Despite a decrease in compression strength with the hybrid scaffolds compared to pure HA scaffolds fabricated by ceramic honeycomb extrusion, the values remain considerably higher than that achieved by traditional fabrication methods, such as direct foaming⁵⁸, polymer replication⁵⁹ and sacrificial templating⁶⁰. The enhanced strengths were attributed to an aligned porous architecture. Other fabrication methods of producing scaffolds with aligned porosity, which resulted in high strength scaffolds, are available, and examples are given in **Table 4**. Hence, there are alternatives to using ceramic extrusion for fabricating BGS. However, ceramic honeycomb extrusion offers speed, low capital and running cost, low skill requirement, and flexibility of altering pore geometry that make it an indispensable fabrication technique⁹.

Ceramic extrusion has been revealed to produce high-strength scaffolds, as demonstrated by both honeycomb and co-extrusion approaches (**Table 4**). The latter encompasses the use of additives, such as camphene, to generate macro-pores. A previous study demonstrated that co-extrusion can produce HA scaffolds with higher compressive strength than honeycomb extrusion⁶¹, however, at a comparable porosity of 55 vol%⁶², the strength was markedly lower (**Table 4**). Thus with respect to achieving a balance between scaffold strength and porosity, honeycomb extrusion is more favourable. With regards to the fabrication process, honeycomb extrusion is once more advantageous. Co-extrusion relies on pore-forming additives to be in their molten state for formulating the ceramic feed. In the case of camphene the feed was processed at 60 °C⁶², and in another study, 105 °C⁶¹ was used. Whereas in honeycomb extrusion ceramic paste formulation, and extrusion thereafter, were performed at

room temperature, thereby obviating the need for high temperatures, and the costs associated therewith. Furthermore, honeycomb ceramic extrusion offers the simplicity of controlling pore geometry by altering die geometry. Roohani-Esfahani et al. (2016)⁶³ demonstrated via robocasting that scaffolds with hexagonal pore geometry yielded the highest compressive strength. A die forming hexagonal pores can be readily manufactured, whereas in co-extrusion the molecular dynamics of, for example, liquid camphene will determine pore geometry. This will require considerable expertise to accomplish.

Unidirectional freeze-casting is another technique capable of achieving high-strength HA scaffolds, as demonstrated by Deville et al. (2006)⁶⁴. In comparison to their approach, honeycomb extrusion is considerably faster, as the process of generating green bodies in the latter is instantaneous; whereas in freeze casting time is needed for freezing the liquid phase. In addition, a sublimation stage is required for generating the pores, which further prolongs the fabrication process with respect to honeycomb extrusion. Furthermore, the preclusion of sub-zero temperature requirements ensures honeycomb extrusion remains comparatively economically viable. Freeze casting has several other limitations that will need to be overcome before scaling up the process⁶⁵, whereas extrusion has been successfully scaled-up for many decades, mainly in the automotive industry. At comparable porosity, Deville et al. (2006) attained a compressive strength of 65 MPa, which is greater than that reported in this study. However, the hybrid scaffolds formed herein comprised of larger macro-pores and a higher bioactive-glass content, hence a superior bioactivity would be expected from the hybrid scaffolds. This is the first study to investigate ceramic-glass hybrids fabricated via honeycomb extrusion, and thus further work is needed to determine whether the compressive strength of the current hybrid scaffolds can be improved. This will include optimisation of particle size, pore geometries and sintering protocol. Furthermore, the scaffolds fabricated herein exhibit

only unidirectional interconnected porosity, whereas freeze-casting possesses both longitudinal and lateral interconnected pores, and thus will need to be addressed in the future.

Robocasting is a relatively new approach to forming porous structure. A similar principle to extrusion is adopted, whereby a ceramic paste is extruded through a nozzle. The nozzle position is pre-determined based on a computer-aided design (CAD), and driven with the same principle used in computer numerical controlled machines to fabricate three-dimensional structures with micrometre resolution⁵. This spatial resolution allows longitudinal and lateral interconnected-pores suitable for BGS to be generated by simply altering the CAD model. Interconnected porosity is a limitation of the scaffolds fabricated in the present study, as the formation thereof require, for example, porogens, which may increase the complexity of the overall fabrication process. Although robocasting is still in its infancy, the results are promising, as reported in **Table 4**. Current drawbacks of the technology are slow speed, high capital costs and a high skill-level is required.

3.3 Cell Viability

In vitro cell viability revealed the hybrid samples to be biocompatible, as illustrated in **Fig. 13**. The MG63 cell lines were used, which are cell lines originating from human bone, and are representative of osteoblastic behaviour. Cell proliferation was observed over a seven-day period. This was believed to be as a result of silicon ion dissolution from the substrates, which has been found to subsequently induce a genetic response for the bone cells to proliferate, as previously discovered⁶⁶. Gene upregulation occurs within 48 hrs⁶⁷, which was sustained for seven days in the present study, despite comprising only 10 wt% of the total hybrid system. In addition, Si dissolution has been found to increase collagen production, which is a component of the organic phase of bone, and hence is required for complete bone restoration⁶⁸.

BG1 and BG2 hybrid exhibited the same increasing trend with time, and thus the substitution of 5 wt% CaO for Na₂O had no effect on the test. It could be contented that a lower Na₂O content decreases glass solubility, thereby reducing Si dissolution and consequently gene upregulation. Although not reported herein, BG2 possessed a higher glass transition temperature (T_g) than BG1, which is a prefigure to solubility (i.e. higher T_g equates to a slower solubility)⁶⁹. In addition, previous work had determined that an increase in sodium oxide in glass results in an increase to cytotoxicity. Hence, the comparable cell viability results of BG1 and BG2 may have occurred due to the aforementioned events offsetting one another. Bellucci et al. (2013)⁴², who compared stoichiometric BG to Ca-excess BG, observed an increase in MC3T3-E1 cell proliferation over time. Initially the Ca-excess BG yielded the higher cell proliferation at day 2, but similar cell proliferation values were observed by day 14. Hence, they too established that Ca-excess BG was not detrimental to cells, and comparable cell viabilities between stoichiometric and Ca-excess BG.

In addition to Bellucci et al., only Lopes and Demirkiran from **Table 5** examined the cell viability of their samples, of which only the latter investigated cell viability at multiple time periods. The studies reported no cytotoxicity when BG was added to their respective calcium phosphate. Demirkiran et al. (2010)²⁸ investigated the DNA concentration, which correlated to the number of bone cells grown, and reported an increase in cell viability with the incorporation of 10 wt% glass from day 3 to day 6. Interestingly, incorporating 5 and 25 wt% BG did not increase cell viability from day 3 to day 6. The authors attributed it to the various chemical compositions obtained post-sintering with each hybrid sample; the 10 wt% composition was the only one to exhibit both a β -TCP and an amorphous phase, which may have synergistically led to an increase in cell viability. Both β -TCP^{70, 71} and an amorphous phase⁷² are known to be more soluble than HA, and hence may have resulted in a higher ion dissolution, and subsequently a higher rate of cell proliferation and surface roughness⁷³.

The CAN hybrid also presented with a similar trend to BG1 and BG2 over seven days. Previous work has also illustrated a similar trend over the course of ten days⁷⁴. At day 7, the cell viability was noticeably higher in CAN than either BG, which can be ascribed to fluoride ions dissolved therefrom. Fluoride ions are one of the most potent stimulators of bone⁷⁵. Previous work by Lee et al. (2006) reported a higher cell viability in HA-bioactive hybrids containing fluorine than fluorine-free hybrids⁷⁶. The next step would be to investigate the biological response in vivo, and determine whether the proliferative behaviour can be translated thereto. A previous in vivo study revealed phosphate-free canasite exhibited no osteoconductivity, and instead favouring soft tissue binding⁷⁷. The authors of that study postulated that the incorporation of phosphate into the glass network may counteract this.

4 Conclusion

Hydroxyapatite-bioactive glass scaffolds have been successfully manufactured using honeycomb extrusion. Three different samples with varying glass composition were produced. The addition of glass induced partial phase transformation of hydroxyapatite to β -tricalcium phosphate during sintering. The bulk porosities and compressive strengths ranged from 55 to 68.6 vol% and 9.8 to 56.7 MPa, respectively, in which increasing the calcium oxide concentration of the raw glass improved scaffold strength. All samples supported cell proliferation over a seven day period, whereby the highest cell viability was obtained at day 7. It is expected that the HA-bioactive glass hybrid scaffolds fabricated via ceramic honeycomb extrusion will provide a possible alternative to commercially available bone graft substitutes comprised of pure HA or HA and bioactive glass.

Acknowledgements

This work was supported by the Department of Mechanical Engineering, University of Sheffield, The Sorby Centre for Electron Microscopy and Microanalysis. The authors would also like to acknowledge Gwendolen C. Reilly Kroto Research Institute and Insigneo Institute for Silico Medicine.

References

1. Giannoudis PV, Dinopoulos H, Tsiridis E. Bone substitutes: an update. *Injury*. 2005;36 Suppl 3:S20-7.
2. Hing KA. Bone repair in the twenty-first century: biology, chemistry or engineering? *Philos. Trans. R. Soc., A*. 2004;362(1825):2821-50.
3. Livingston T, Ducheyne P, Garino J. In vivo evaluation of a bioactive scaffold for bone tissue engineering. *J. Biomed. Mater. Res.* 2002;62(1):1-13.
4. Barriga A, Díaz-de-Rada P, Barroso JL, Alfonso M, Lamata M, Hernáez S, et al. Frozen cancellous bone allografts: positive cultures of implanted grafts in posterior fusions of the spine. *European Spine Journal*. 2004;13(2):152-6.
5. M. Elbadawi JM, L. Hopkins and I. Reaney. Progress in Bioactive Metal and, Ceramic Implants for Load- Bearing Application. In: Zorzi, AR, Miranda JBd, editors. *Advanced Techniques in Bone Regeneration* 2016.
6. Dorozhkin SV. Bioceramics of calcium orthophosphates. *Biomaterials*. 2010;31(7):1465-85.
7. O'Brien FJ. Biomaterials & scaffolds for tissue engineering. *Mater. Today*. 2011;14(3):88-95.
8. Meredith J, Mallick KK. High-strength scaffolds for bone regeneration. *Bioinspired, Biomimetic Nanobiomater*. 4(1):48-58.
9. Händle F. *Extrusion in Ceramics*. Berlin, Heidelberg: Springer Berlin Heidelberg; 2007.
10. Feng S, He F, Ye J. Fabrication and characterization of honeycomb β -tricalcium phosphate scaffolds through an extrusion technique. *Ceram. Int*. 2017;43(9):6778-85.
11. Bellucci D, Sola A, Cannillo V. Hydroxyapatite and tricalcium phosphate composites with bioactive glass as second phase: State of the art and current applications. *J. Biomed Mater. Res., Part A*. 2016;104(4):1030-56.
12. Lopes JH, Magalhães JA, Gouveia RF, Bertran CA, Motisuke M, Camargo SEA, et al. Hierarchical structures of β -TCP/45S5 bioglass hybrid scaffolds prepared by gelcasting. *J. Mech. Behav. Biomed. Mater.* 2016;62:10-23.
13. Yazdanpanah Z, Bahrololoom ME, Hashemi B. Evaluating morphology and mechanical properties of glass-reinforced natural hydroxyapatite composites. *J. Mech. Behav. Biomed. Mater.* 2015;41(0):36-42.
14. Lin K, Chang J, Liu Z, Zeng Y, Shen R. Fabrication and characterization of 45S5 bioglass reinforced macroporous calcium silicate bioceramics. *J. Eur. Ceram. Soc.* 2009;29(14):2937-43.
15. Knowles JC, Talal S, Santos JD. Sintering effects in a glass reinforced hydroxyapatite. *Biomaterials*. 1996;17(14):1437-42.

16. Tancred DC, McCormack BAO, Carr AJ. A quantitative study of the sintering and mechanical properties of hydroxyapatite/phosphate glass composites. *Biomaterials*. 1998;19(19):1735-43.
17. Santos JD, Reis RL, Monteiro FJ, Knowles JC, Hastings GW. Liquid phase sintering of hydroxyapatite by phosphate and silicate glass additions: structure and properties of the composites. *J Mater Sci: Mater Med*. 1995;6(6):348-52.
18. Baino F, Verné E, Vitale-Brovarone C. 3-D high-strength glass–ceramic scaffolds containing fluoroapatite for load-bearing bone portions replacement. *Mater. Sci. Eng., C*. 2009;29(6):2055-62.
19. Bhakta S, Faira PE, Salata LA, de Oliveira Neto PJ, Miller CA, van Noort R, et al. Determination of relative in vivo osteoconductivity of modified potassium fluorrichterite glass–ceramics compared with 45S5 bioglass. *J Mater Sci: Mater Med*. 2012;23(10):2521-9.
20. Georgiou G, Knowles JC. Glass reinforced hydroxyapatite for hard tissue surgery—Part 1: mechanical properties. *Biomaterials*. 2001;22(20):2811-5.
21. Elbadawi M, Mosalagae M, Reaney IM, Meredith J. Guar gum: A novel binder for ceramic extrusion. *Ceram Int*. 2017;43(18):16727-35.
22. Webb PAaO, C. *Analytical Methods in Fine Particle Technology*. Norcross, GA USA: Micromeritics instrument corp; 1997.
23. Elbadawi M, Meredith J, Mosalagae M, Reaney IM. Porous hydroxyapatite scaffolds fabricated from nano-sized powder via honeycomb extrusion. *Adv. Mater. Lett*. 2017.
24. Guillon O, Cao S, Chang J, Wondraczek L, Boccaccini AR. Effect of uniaxial load on the sintering behaviour of 45S5 Bioglass® powder compacts. *J. Eur. Ceram. Soc*. 2011;31(6):999-1007.
25. Hill R. An alternative view of the degradation of bioglass. *J. Mater. Sci. Lett*. 1996;15(13):1122-5.
26. Brauer DS, Mneimne M, Hill RG. Fluoride-containing bioactive glasses: Fluoride loss during melting and ion release in tris buffer solution. *J. Non-Cryst. Solids*. 2011;357(18):3328-33.
27. Shelby JE. *Introduction to glass science and technology*. 2nd ed. ed. Cambridge: Cambridge : Royal Society of Chemistry, c2005; 2005.
28. Demirkiran H, Mohandas A, Dohi M, Fuentes A, Nguyen K, Aswath P. Bioactivity and mineralization of hydroxyapatite with bioglass as sintering aid and bioceramics with Na₃Ca₆(PO₄)₅ and Ca₅(PO₄)₂SiO₄ in a silicate matrix. *Mater. Sci. Eng. C*. 2010;30(2):263-72.
29. Santos JD, Knowles JC, Reis RL, Monteiro FJ, Hastings GW. Microstructural characterization of glass-reinforced hydroxyapatite composites. *Biomaterials*. 1994;15(1):5-10.
30. Wang L-L, Wang X-F, Ding X, Jiang H-T. Preparation of HA-Bioglass-Al₂O₃ Biological Composite. *Mater. Manuf. Processes*. 2013;28(9):980-3.
31. Atayde LM, Cortez PP, Afonso A, Santos M, Maurício AC, Santos JD. Morphology effect of bioglass-reinforced hydroxyapatite (Bonelike®) on osteoregeneration. *J. Biomed. Mater. Res., Part B*. 2015;103(2):292-304.
32. Ou S-F, Chiou S-Y, Ou K-L. Phase transformation on hydroxyapatite decomposition. *Ceram. Int*. 2013;39(4):3809-16.
33. Carrodeguas RG, De Aza S. α -Tricalcium phosphate: Synthesis, properties and biomedical applications. *Acta Biomater*. 2011;7(10):3536-46.
34. Siqueira L, Passador FR, Costa MM, Lobo AO, Sousa E. Influence of the addition of β -TCP on the morphology, thermal properties and cell viability of poly (lactic acid) fibers obtained by electrospinning. *Mater. Sci. Eng. C*. 2015;52:135-43.

35. Moreira APD, Sader MrS, Soares GDdA, Leao MHMR. Strontium Incorporation on Microspheres of Alginate/ β -tricalcium Phosphate as Delivery Matrices. *Mat. Res.* 2014;17:967-73.
36. Pramanik S, Agarwal AK, Rai KN, Garg A. Development of high strength hydroxyapatite by solid-state-sintering process. *Ceram. Int.* 2007;33(3):419-26.
37. Karageorgiou V, Kaplan D. Porosity of 3D biomaterial scaffolds and osteogenesis. *Biomaterials.* 2005;26(27):5474-91.
38. Klein CPAT, de Groot K, Drissen AA, van der Lubbe HBM. Interaction of biodegradable β -whitlockite ceramics with bone tissue: An in vivo study. *Biomaterials.* 1985;6(3):189-92.
39. Trunec M, Chlup Z. Subtractive manufacturing of customized hydroxyapatite scaffolds for bone regeneration. *Ceram. Int.*
40. Chen Z, Zhang X, Yang Y, Zhou K, Wragg N, Liu Y, et al. Fabrication and characterization of 3D complex hydroxyapatite scaffolds with hierarchical porosity of different features for optimal bioactive performance. *Ceram. Int.* 2017;43(1, Part A):336-44.
41. Rahaman MN. *Ceramic Processing and Sintering.* Florida: Taylor & Francis Group; 2003.
42. Bellucci D, Sola A, Gazzarri M, Chiellini F, Cannillo V. A new hydroxyapatite-based biocomposite for bone replacement. *Mater. Sci. Eng. C.* 2013;33(3):1091-101.
43. Gibson IR, Best SM, Bonfield W. Effect of Silicon Substitution on the Sintering and Microstructure of Hydroxyapatite. *J. Am. Ceram. Soc.* 2002;85(11):2771-7.
44. Kim SR, Lee JH, Kim YT, Riu DH, Jung SJ, Lee YJ, et al. Synthesis of Si,Mg substituted hydroxyapatites and their sintering behaviors. *Biomaterials.* 2003;24(8):1389-98.
45. Tancred DC, Carr AJ, McCormack BAO. The sintering and mechanical behavior of hydroxyapatite with bioglass additions. *J Mater Sci: Mater Med.* 2001;12(1):81-93.
46. Elbadawi M, Shbeh M. High strength yttria-reinforced HA scaffolds fabricated via honeycomb ceramic extrusion. *J. Mech. Behav. Biomed. Mater.* 2018;77(Supplement C):422-33.
47. Kurien T, Pearson RG, Scammell BE. Bone graft substitutes currently available in orthopaedic practice The evidence for their use. *The bone and Joint Journal.* 2013;95-B(5):583-97.
48. Goller G, Demirkiran H, Oktar FN, Demirkesen E. Processing and characterization of bioglass reinforced hydroxyapatite composites. *Ceram. Int.* 2003;29(6):721-4.
49. Kapoor S, Batra, U. Preparation and Bioactivity Evaluation of Bone like Hydroxyapatite - Bioglass Composite. *Conference Preceedings.* 2010; 4(1)37-41.
50. Gutierrez M, Lopes MA, Sooraj Hussain N, Lemos AF, Ferreira JMF, Afonso A, et al. Bone ingrowth in macroporous Bonelike® for orthopaedic applications. *Acta Biomater.* 2008;4(2):370-7.
51. Silva MHPd, Lemos AF, Ferreira JMdF, Santos JD. Mechanical characterisation of porous glass reinforced hydroxyapatite ceramics: Bonelike®. *Mat. Res.* 2003;6:321-5.
52. Elbadawi M, Shbeh M. High Strength Yttria-reinforced HA scaffolds fabricated via Honeycomb Ceramic Extrusion. *J. Mech. Behav. Biomed. Mater.* 2018;77:422-433.
53. Shuai C, Li P, Liu J, Peng S. Optimization of TCP/HAP ratio for better properties of calcium phosphate scaffold via selective laser sintering. *Mater. Charact.* 2013;77:23-31.
54. Houmard M, Fu Q, Genet M, Saiz E, Tomsia AP. On the structural, mechanical, and biodegradation properties of HA/ β -TCP robocast scaffolds. *J. Biomed. Mater. Res., Part B.* 2013;101(7):1233-42.
55. Sprio S, Tampieri A, Celotti G, Landi E. Development of hydroxyapatite/calcium silicate composites addressed to the design of load-bearing bone scaffolds. *J. Mech. Behav. Biomed. Mater.* 2009;2(2):147-55.

56. Beheri HH, Mohamed KR, El-Bassyouni GT. Mechanical and microstructure of reinforced hydroxyapatite/calcium silicate nano-composites materials. *Mater. Des.* 2013;44:461-8.
57. Desogus L, Cuccu A, Montinaro S, Orrù R, Cao G, Bellucci D, et al. Classical Bioglass® and innovative CaO-rich bioglass powders processed by Spark Plasma Sintering: A comparative study. *J. Eur. Ceram. Soc.* 2015;35(15):4277-85.
58. Zhang L-y, Zhou D-l, Chen Y, Liang B, Zhou J-b. Preparation of high open porosity ceramic foams via direct foaming molded and dried at room temperature. *J. Eur. Ceram. Soc.* 2014;34(10):2443-52.
59. Yook S-W, Kim H-E, Yoon B-H, Soon Y-M, Koh Y-H. Improvement of compressive strength of porous hydroxyapatite scaffolds by adding polystyrene to camphene-based slurries. *Mater. Lett.* 2009;63(11):955-8.
60. Wu J, Ruan C, Ma Y, Wang Y, Luo Y. Vital role of hydroxyapatite particle shape in regulating the porosity and mechanical properties of the sintered scaffolds. *J. Mater. Sci. Technol.* 2017.
61. Koh Y-H, Kim H-W, Kim H-E, Halloran JW. Fabrication of Macrochannelled-Hydroxyapatite Bioceramic by a Coextrusion Process. *J. Am. Ceram. Soc.* 2002;85(10):2578-80.
62. Choi W-Y, Kim H-E, Moon Y-W, Shin K-H, Koh Y-H. Production of porous Calcium Phosphate (CaP) ceramics with aligned pores using ceramic/camphene-based co-extrusion. *Biomater. Res.* 2015;19:16.
63. Roohani-Esfahani S-I, Newman P, Zreiqat H. Design and Fabrication of 3D printed Scaffolds with a Mechanical Strength Comparable to Cortical Bone to Repair Large Bone Defects. *Sci. Rep.* 2016;6:19468.
64. Deville S, Saiz E, Tomsia AP. Freeze casting of hydroxyapatite scaffolds for bone tissue engineering. *Biomaterials.* 2006;27(32):5480-9.
65. Deville S. Freeze-Casting of Porous Ceramics: A Review of Current Achievements and Issues. *Adv. Eng. Mater.* 2008;10(3):155-69.
66. Hench LL, Jones JR. Bioactive Glasses: Frontiers and Challenges. *Front. Biong. Biotechnol.* 2015;3:194.
67. Xynos ID, Edgar AJ, Buttery LDK, Hench LL, Polak JM. Gene-expression profiling of human osteoblasts following treatment with the ionic products of Bioglass® 45S5 dissolution. *J. Biomed. Mater. Res.* 2001;55(2):151-7.
68. Helen W, Gough JE. Cell viability, proliferation and extracellular matrix production of human annulus fibrosus cells cultured within PDLLA/Bioglass® composite foam scaffolds in vitro. *Acta Biomater.* 2008;4(2):230-43.
69. Wallace K, Hill R, Pembroke J, Brown C, Hatton P. Influence of sodium oxide content on bioactive glass properties. *J Mater Sci: Mater Med.* 1999;10(12):697-701.
70. Klein CPAT, de Blic-Hogemrst JMA, Wolket JGC, de Groot K. Studies of the solubility of different calcium phosphate ceramic particles in vitro. *Biomaterials.* 1990;11(7):509-12.
71. Lind M, Overgaard S, Bünger C, Søballe K. Improved bone anchorage of hydroxyapatite coated implants compared with tricalcium-phosphate coated implants in trabecular bone in dogs. *Biomaterials.* 1999;20(9):803-8.
72. Ghomi H, Fathi MH, Edris H. Effect of the composition of hydroxyapatite/bioactive glass nanocomposite foams on their bioactivity and mechanical properties. *Mater. Res. Bull.* 2012;47(11):3523-32.
73. Ogata K, Imazato S, Ehara A, Ebisu S, Kinomoto Y, Nakano T, et al. Comparison of osteoblast responses to hydroxyapatite and hydroxyapatite/soluble calcium phosphate composites. *J. Biomed. Mater. Res., Part A.* 2005;72A(2):127-35.

74. Liporaci JLJ, Rosa AL, Beloti MM, Johnson A, van Noort R, da Rocha Barros VM. In vitro osteogenesis on fluorcanasite glass-ceramic with three different chemical compositions. *J Mater Sci: Mater Med.* 2007;19(2):833.
75. Farley JR, Wergedal JE, Baylink DJ. Fluoride Directly Stimulates Proliferation and Alkaline Phosphatase Activity of Bone-Forming Cells. *Science.* 1983;222(4621):330-2.
76. Lee E-J, Chae S-Y, Kim H-E, Kim H-W. Improvement in Biocompatibility of Fluoridated Apatite with Addition of Resorbable Glass. *J. Am. Ceram. Soc.* 2006;89(5):1748-51.
77. da Rocha Barros VM, Salata LA, Sverzut CE, Xavier SP, van Noort R, Johnson A, et al. In vivo bone tissue response to a canasite glass-ceramic. *Biomaterials.* 2002;23(14):2895-900.
78. Dellinger JG, Wojtowicz AM, Jamison RD. Effects of degradation and porosity on the load bearing properties of model hydroxyapatite bone scaffolds. *J. Biomed. Mater. Res., Part A.* 2006;77(3):563-71.
79. Calori GM, Mazza E, Colombo M, Ripamonti C. The use of bone-graft substitutes in large bone defects: Any specific needs? *Injury.* 2011;42, Supplement 2:S56-S63.

Tables

Table 1.

Glass composition of CAN, BG1 and BG2 in mass%.

Glass Compound	CAN mass%	BG1 mass%	BG2 mass%
SiO ₂	58.4	45	45
P ₂ O ₅	4.6	6	6
Na ₂ O	3.7	24.5	19.5
CaO	15.5	24.5	29.5
K ₂ O	7.6	-	-
CaF ₂	10.2	-	-

Table 2.

Paste Composition for all hybrid formulations in grams.

Component	Weight (g)
HA	217
Bioactive Glass	24
Methocel®	18
Distilled Water	100

Table 3.

Particle Properties of the raw glass powders.

Sample	Particle Size (µm)			Powder density (g/cm ³)	BET Surface area (m ² /g)
	D ₁₀	D ₅₀	D ₉₀		
BG1	3.24	13.8	27.6	2.75 ± 0.010	3.10 ± 0.138
BG2	1.72	8.81	21.4	2.73 ± 0.002	3.57 ± 0.118
CAN	2.31	16.2	45.1	2.63 ± 0.004	2.25 ± 0.070

Table 4.

Examples of fabrication techniques that produce aligned porous structures, and their respective porosity and compressive strength. (* proprietary glass)

Technique	Material	Macro-pore size (µm)	Porosity (vol%)	Compressive strength (MPa)
Ceramic honeycomb extrusion ⁴⁶	HA	~750	45	105.9
Ceramic co-extrusion ⁶¹	HA	270	27	240
Ceramic co-extrusion ⁶²	HA	~35	55	19.3
Freeze-casting ⁶⁴	HA	< 600	56	65
Robocasting ⁷⁸	HA	~300	~50	140
Robocasting ^{63, 79}	Sr-HT* glass	~900	~60	139

Table 5.

Examples of calcium phosphate-bioactive glass hybrids, and their respective bioactive glass composition, sintering temperature, dwell time, decomposition products and final density relative to pure calcium phosphate. (HA- hydroxyapatite; BG-Bioglass®; TCP- tricalcium phosphate; CaSiO – calcium silicate; Si-HA – silicon substituted hydroxyapatite)

Study	Starting Hybrid	Glass mass%	Sintering (°C)	Dwell time (h)	Products	Density relative to pure CaP
Santos ²⁹	HA/BG	5	1200-1300	1	α -TCP, β -TCP, Si-HA	Decreased
Bellucci ⁴²	HA/BG_Ca	40	1150	3	HA	Decreased ^a
Lopes ¹²	TCP/BG	7.5	1200	2	α -TCP, β -TCP	No change
Goller ⁴⁸	HA/BG	10	1200 & 1300	4	Si-HA, Ca ₂ P ₂ O ₇ , Na ₂ HPO ₄	N/A
Yazdanpanah ¹³	HA/Sodalime glass	5	800-1200	2	HA	Decreased
Lin ¹⁴	CaSiO/BG	5	1100	3	CaSiO	Increased
Knowles ¹⁵	HA/Na ₂ -CaO-P ₂ O ₅	2	1200-1350	1	HA	No Change
	HA/Na ₂ -CaO-P ₂ O ₅	4	1200-1350	1	α -TCP, β -TCP, HA	Decreased
Tancred ¹⁶	HA/Phosphate glass	10	1150-1350	3	α -TCP, β -TCP, HA	Decreased
Tancred ⁴⁵	HA/BG	2.5-50	1050-1200	3	β -TCP, HA	Decreased
Demirkiran ²⁸	HA/BG	10	1200	4	Si-HA, β -TCP	Decreased

^a Relative to a hybrid comprised of HA and stoichiometric BG

Figures

Fig. 1. SEM (SE) micrographs representation depictions of the Bioglass (top) and canasite (bottom) raw powders.

Fig. 2. XRD analysis of the raw glass powders.

Fig. 3. FTIR spectra of the raw powders.

Fig. 4. STA analysis depicting the DSC (a) and TGA (b) thermograms of the raw bioactive glass powders.

Fig. 5. Images of a sintered CAN extrudate, using an optical (a), SEM (SE) (b) and camera (c).

Fig. 6. XRD patterns of BG1 and BG2 sintered at different temperatures.

Fig. 7. XRD pattern of CAN scaffolds sintered at 1250 and 1300 °C.

Fig. 8. FTIR spectra of BG1 and BG2 at different sintering temperatures.

Fig. 9. FTIR spectra of HA-CAN sintered at 1250 and 1300 °C.

Fig. 10. HA-bioactive glass bulk porosities (n = 3) (a) and compressive strength (loading performed parallel to cell alignment) (n = 9) (b) values.

Fig. 11. SEM (SE) micrographs depicting the fracture surface of BG1 (top) and BG2 (bottom), at 1200 (left), 1250 (middle) and 1300 °C (right).

Fig. 12. SEM (SE) micrographs depicting the fracture surface of CAN at 1300 °C.

Fig. 13. Cell Viability of BG1 and BG2 at 1200 and 1250 °C; CAN at 1300 °C.